*Korean J. Chem. Eng.*, 37(3), 448-455 (2020)
DOI: 10.1007/s11814-019-0469-6

pISSN: 0256-1115
eISSN: 1975-7220

# Synthesis of $MoO_x$ nanostructures with the assistance of polymeric surfactants for dye removal from water

**Nemat Tahmasebi† and Marzieh Khalildashti**

Department of Physics, Jundi-Shapur University of Technology, Dezful, Iran
(*Received 5 September 2019 • accepted 21 December 2019*)

**Abstract**−$MoO_3$ and reduced molybdenum oxides ($MoO_x$, x=2.87 and 2) were successfully synthesized through a one-pot hydrothermal method without and with adding polymeric surfactants (PVP or PVA) as capping and reducing agents into the reaction solution. The synthesized nanostructures were characterized by different techniques. Adding polymeric surfactants into hydrothermal reaction solution had significant effect on the structural, optical and morphological properties of products. Orthorhombic phase of $MoO_3$ nanorods, monoclinic phase of $MoO_{2.87}$ nanoparticles and monoclinic phase of $MoO_2$ nanoparticles were obtained in the absence and in the presence of PVP and PVA, respectively. The specific surface area of $MoO_3$, $MoO_{2.87}$ and $MoO_2$ samples calculated by the BET method was found to be 15.64, 5.94 and 87.62 $m^2g^{-1}$, respectively. The dye adsorption capability of products was investigated for removal of RhB molecules from water. The experimental results indicated that the RhB adsorption on $MoO_2$ is much faster and higher than that of $MoO_3$ and $MoO_{2.87}$, which can be attributed to the larger specific surface area. Furthermore, the kinetic models and isotherm models were studied to determine the adsorption rate and mechanism of RhB adsorption onto the products.

Keywords: Hydrothermal, Nanoparticles, Molybdenum Oxide, Surfactant, Water Treatment

## INTRODUCTION

With the rapid development of industries, water pollution has become a common environmental problem in all the world. Every year, high amount of organic dyes ($7\times10^5$ tyear$^{-1}$) from textiles, paints, leathers and paper industrials is discharged into water [1-3]. Most of the dyes are quite toxic and chemically stable and may cause problems for human health [4,5]. Therefore, the removal of organic pollutants from water has received much research interest. Various techniques such as precipitation, ozone, ultrafiltration, photocatalysis and adsorption have been studied for water treatment [6-10]. Among them, adsorption is a simple and most popular method to remove the contaminants from water due to its high efficiency, relatively low cost, ease of separation and environmentally friendly nature, which is extensively applied in water treatment [11-14]. In recent years, the use of metal oxides, including $WO_3$, $ZnCo_2O_4$, and $TiO_2$ as adsorbent for dye removal from wastewater, has received much research interest because of high specific surface area, and also unique physical and chemical properties [15-18].

Molybdenum oxide is a common metal oxide which exists in various compositions ranging from fully stoichiometric molybdenum oxide ($MoO_3$) to partially reduced $MoO_{3-x}$ (2<x<3) and significantly reduced molybdenum dioxide ($MoO_2$) [19]. $MoO_3$ is an n-type semiconductor with a wide band gap of 3.2 eV, which its band gap decreases in the presence of oxygen vacancies ($MoO_{3-x}$) [19,20]. In contrast, the metallic characteristics of $MoO_2$ are stronger than its semiconductor properties due to large amount of free electrons induced by oxygen vacancies [19,21]. Recently, molybdenum dioxide ($MoO_2$) as a conductive metal oxide has attracted great attention for practical application in many fields such as Li-ion batteries, supercapacitor, photothermal, photocatalyst and adsorption, due to its low electrical resistivity, high melting point, low cost, non-toxicity and high chemical stability [22-26].

Up to now, few studies about the dye adsorption properties of molybdenum oxide have been reported. Wang et al. reported that the 3D hierarchical architecture of $MoO_3$ exhibits a fast and selective adsorption to adsorb organic pollutants with benzoic acidic group [14]. Hu et al. prepared $MoO_2$ hollow microspheres which exhibit fast adsorption rate and high removal of Cr (VI) from water due to the large surface area (37.7 $m^2$/g) and mesoporous structure [25]. Cao et al. prepared $MoO_3$ nanowires with large specific surface area (174.7 $m^2$/g) in the presence of $Fe^{3+}$ cations, which show excellent and highly selective adsorption capacity toward quasi-phenothiazine dyes [27]. In spite of these efforts, in comparison with other metal oxides such as ZnO, $TiO_2$ and $WO_3$, $MoO_x$ is in the early stages and more attempts are still needed to optimize its use for its practical application as adsorbent for dye removal from water.

On the other hand, it is widely known that nanostructured materials display distinct physical and chemical properties compared with their bulk, due to the higher surface to value molar ratio and larger specific surface area. Moreover, the properties of nanostructured materials are strongly sensitive to the size and shape dependent [28,29]. Up to now, several different methods such as solid state reaction, solvothermal and hydrothermal have been used to synthesize variety of molybdenum oxide nanostructures including nanosheets, nanorods, nanoparticles, and nanospheres. In this work, a facile one-step hydrothermal method was used to synthesize stoichiometric and reduced molybdenum oxide nanostructures without and with the assistance of polymeric surfactants (PVP or PVA) as capping and reducing agents. Then, the dye adsorption capability

†To whom correspondence should be addressed.
E-mail: tahmasebi@jsu.ac.ir
Copyright by The Korean Institute of Chemical Engineers.

of synthesized $MoO_x$ (X=3, 2.87 and 3) nanostructures was investigated for removal of organic dyes from water.

## EXPERIMENTAL

### 1. Synthesis

All reagents were analytical grade and used without further purification. $MoO_2$ (or $MoO_{2.87}$) nanoparticles were synthesized as follows: 1.20 g of $Na_2MoO_4$ was added into 50 ml distilled water under continues stirring for 70 min, which was named as solution 1. Then, 0.40 g polyvinyl alcohol (PVA, MW=60,000) (or polyvinylpyrrolidone (PVP, MW=1,300,000)) and 1.60 ml HCl were dissolved in 50 ml of distilled water at temperature of 80 °C under magnetic stirring for 25 min to obtain solution 2. Subsequently, solution 1 drop by drop was added into solution 2 under magnetic stirring. Finally, 80 ml of the mixed solution was loaded into a 100 ml Teflon-lined stainless steel autoclave. The autoclave was maintained at 180 °C for 12 h. The solution chamber was cooled to room temperature, the obtained black powder was collected by centrifugation and washed with distilled water for three times and then dried in an oven at 80 °C for 4 h. $MoO_3$ nanorods were also prepared with the same synthesis procedure in the absence of surfactant within the hydrothermal reaction solution.

### 2. Characterization

The crystal structure of the products was studied by X-ray diffraction (XRD, Philips-PW1730 model) by using Cu K$\alpha$ radiation (($\lambda$=1.54178 Å). Field emission scanning electron microscopy (FESEM, TESCAN-MIRA III model) was used to characterize the morphology of products. Fourier transform infrared (FTIR) spectra of the products were recorded using a Thermo-Avatar. Ultraviolet-visible diffuse reflectance spectra (UV-Vis DRS) were collected on an Avaspec-2048-TEC spectrometer by using $BaSO_4$ as a reference. The Brunauer-Emmet-Teller (BET) surface area was determined from $N_2$ adsorption-desorption at 77 K using a BEL-BELSORP MINI II analyzer. Zeta potential was measured using zeta potential analyzer (Malvern; ZEN3600).

### 3. Adsorption Experiments

To investigate the adsorption properties of synthesized nanostructures, 45 mg of the products was added into 45 ml of RhB aqueous solution (40 mg/*l*) in the dark condition under magnetic stirring. After adsorption, the suspension was centrifuged to remove sample particles, and the concentration of residual RhB solution was analyzed by determining the maximum absorption of RhB at 554 nm using UV-Vis spectrometer. The percent removal of dye molecules from aqueous solution was determined by the following equation:

$$\% \text{ Removal} = \frac{C_0 - C_e}{C_0} \times 100 \quad (1)$$

where $C_0$ and $C_e$ are the initial and final concentration (mg/L) of the dyes, respectively. The adsorption amount (mg/g) at different times was calculated as below:

$$q_t = \frac{(C_0 - C_t) \times V}{m} \quad (2)$$

where $C_0$ and $C_t$ are the concentration of dye (mg/L) at initial time and at different times, respectively, V (L) is the volume of dye solution and m (g) is the amount of adsorbent. For the equilibrium adsorption measurement, 10 mg of the products was added into 40 ml of RhB aqueous solution with initial concentration of 5-200 mg/L, then the solution was stirred in dark condition for 16 h. Furthermore, the adsorption performance of $MoO_2$ nanoparticles to remove other organic dyes (methylene blue (MB), malachite green (MG), methyl orange (MO) and tartrazine (TRT)) from aqueous solution (10 mg/L) was carried out in the same experimental condition with the kinetic adsorption of RhB.

## RESULTS AND DISCUSSION

### 1. Materials Characterization

Fig. 1 shows the XRD patterns of hydrothermally synthesized products without and with adding different surfactants (PVP or PVA) into the reaction solution. In the case of surfactant-free sample, all the diffraction peaks can well be indexed to the orthorhombic crystal phase of $MoO_3$ (JCPDS No. 01-0706) with the lattice parameters of a=3.9450 Å, b=13.8250 Å, c=3.6940 Å and $\alpha=\beta=\gamma=90^o$. The crystal structure of synthesized sample in the presence of PVP can be ascribed to the monoclinic phase of $MoO_{2.87}$ (JCPDS No. 05-0339) with the lattice parameters of a=16.90 Å, b=4.05 Å, c=13.38 Å and $\alpha=\gamma=90.00^o$ and $\beta=106.40^o$. In addition, in the case of synthesized sample with the assistance of PVA, all the diffraction peaks can well be indexed to the monoclinic phase of $MoO_2$ (JCPDS No. 32-0671) with the lattice parameters

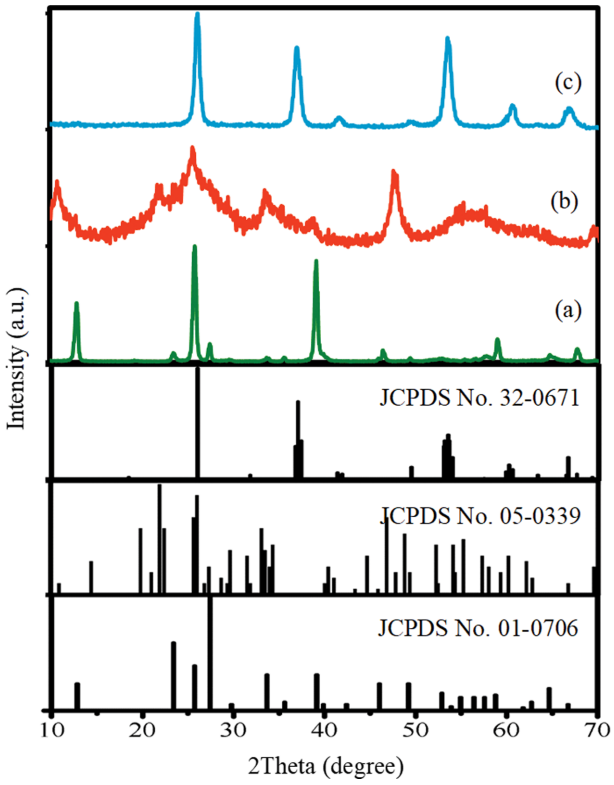



**Fig. 1. XRD patterns of hydrothermally synthesized products (a) without, and with adding (b) PVP and (c) PVA as surfactant into the reaction solution.**

of a=5.60 Å, b=4.85 Å, c=5.53 Å and $\alpha=\gamma=90.00^{o}$ and $\beta=119.37^{o}$. As reported in the literature, polymers with hydroxyl (-OH) end groups can act as reducing agents, and the reducing ability is proportional to the number of hydroxyl (-OH) end groups [28-30]. In this work, the XRD results confirmed that the PVP and PVA can reduce the molybdenum ions with the help of OH groups. However, our observation indicated that the reducing power of PVP is lower than that of PVA, which is suggested to be due to the number of available hydroxyl end groups of PVA in comparison to PVP.

FTIR spectra were used to determine the chemical bonds and the surface functional groups. FTIR spectrum of $MoO_3$ nanorods is displayed in Fig. 2(a). The absorption bands in the range of 500-1,000 $cm^{-1}$ are characteristic of the metal - oxygen bonds [31,32]. The bands located at 995 $cm^{-1}$, 864 $cm^{-1}$ and 561 $cm^{-1}$ can be attributed to the terminal Mo=O stretching vibration mode, the stretching vibration of oxygen in Mo-O-Mo bond, and the bending vibration of oxygen atom linked to three Mo atoms [31,32]. Fig. 2(b)

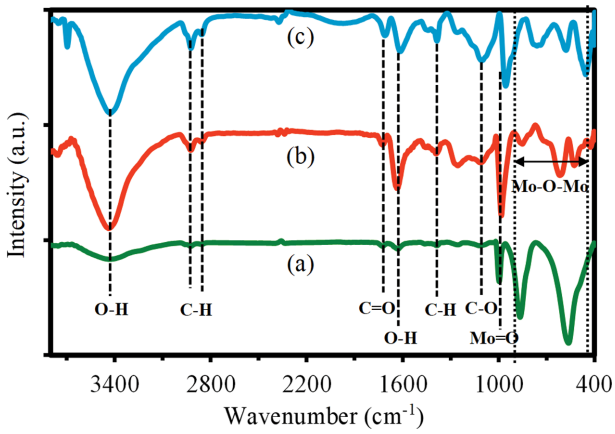



**Fig. 2. FTIR spectra of hydrothermally synthesized products (a) without, and with adding (b) PVP and (c) PVA as surfactant into the reaction solution.**

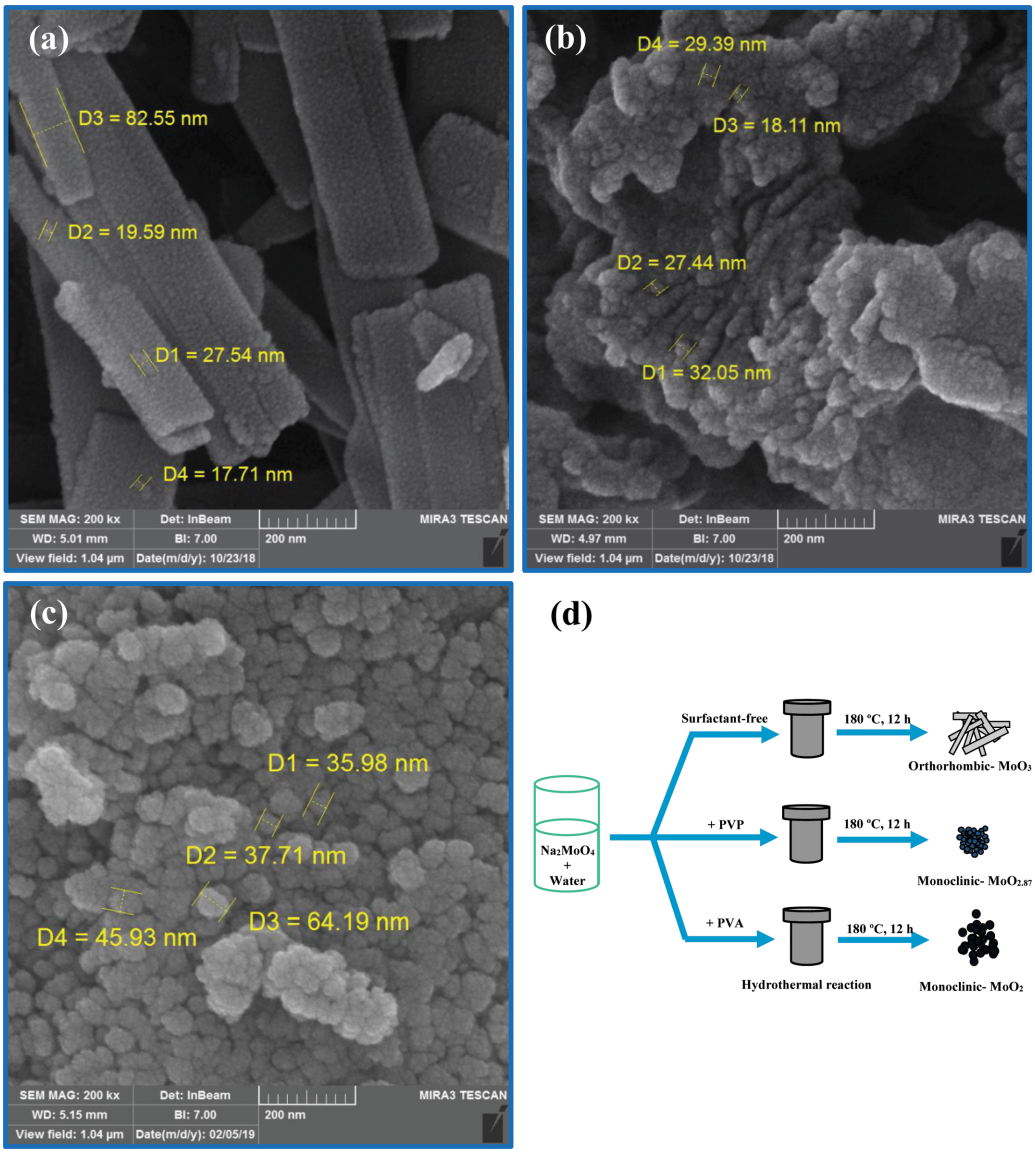



**Fig. 3. FESEM images of (a) $MoO_3$, (b) $MoO_{2.87}$, (c) $MoO_2$ and (d) schematic illustration of synthesized products.**

and (c) show the FTIR spectrum of $MoO_{2.87}$ and $MoO_2$ samples, respectively. The absorption bands in the range of 500-880 $cm^{-1}$ are the characteristic bands of Mo-O-Mo stretching vibration, and the absorption bands at about 950-1,000 $cm^{-1}$ are assigned to the characteristic mode of Mo=O [19,25]. It is observed the absorption band of Mo=O for $MoO_3$ sample has shifted from 990 to 981 $cm^{-1}$ and 952 $cm^{-1}$ for $MoO_{2.87}$ and $MoO_2$ samples, respectively, which can be attributed to the formation of Mo-O…H bonds. It is expected the H atoms in polymer chain (PVP or PVA) covalently bond to O atoms in Mo=O bonds [33]. Furthermore, the bands at about 1,620 and 3,421 $cm^{-1}$ are attributed to the bending and stretching vibrations of O-H bonds of adsorbed water [34]. The observed bands at 2,921 $cm^{-1}$, 1,704 $cm^{-1}$, 1,385 $cm^{-1}$ and 1,099 $cm^{-1}$ can be ascribed to the asymmetric stretching vibration of C-H, vibration of C=O bonds, C-H bending vibration and C-O stretching of acetyl groups, respectively [35,36]. As a consequence, the FTIR results indicate the surface functionalization of $MoO_{2.87}$ and $MoO_2$ by PVP and PVA, respectively.

Fig. 3(a)-(b) shows the FE-SEM images of synthesized products in the absence and in the presence of PVP and PVA as surfactant. It can be seen the rod-shape particles are formed without surfactant (Fig. 3(a)). The average diameter and length of nanorods are ~200 nm and ~700 nm, respectively. According to Fig. 3(b), the FE-SEM image of synthesized sample in the presence of PVP consists mostly of nanoparticles in the range of 20-30 nm. Meanwhile, the FE-SEM image of synthesized sample in the presence of PVA indicates that the sample is composed of nearly uniform spherical nanoparticles that range around 35 to 65 nm. It is suggested the polymeric chains of surfactants adsorbed on particles surface as a capping agents and controlled the shape of the products. Based on above-mentioned experimental data, a simplified schematic illustration of synthesized products without and with the assistance of PVP and PVA is proposed and shown in Fig. 3(d).

The UV-Vis diffuse reflectance spectra of the $MoO_3$, $MoO_{2.87}$ and $MoO_2$ samples are displayed in Fig. 4. It is observed the $MoO_3$ and $MoO_{2.87}$ absorb UV light and display low absorption in visible and NIR regions. Moreover, the absorption edges are around 435 nm, which is the characteristic of wide band-gap semiconductors. In contrast, the $MoO_2$ exhibits a broad light absorption from

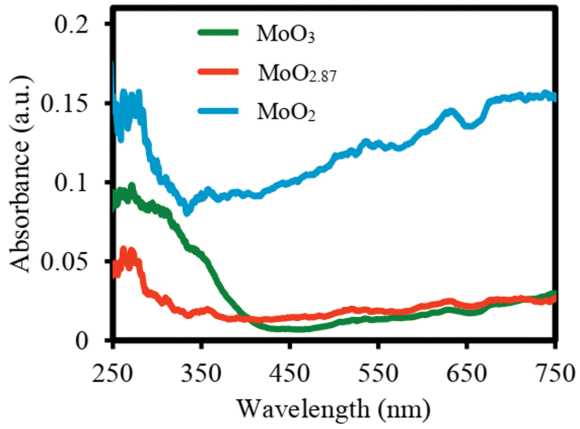



**Fig. 4. UV-Vis absorption spectra of (a) $MoO_3$, (b) $MoO_{2.87}$, (c) and (d) $MoO_2$ samples.**

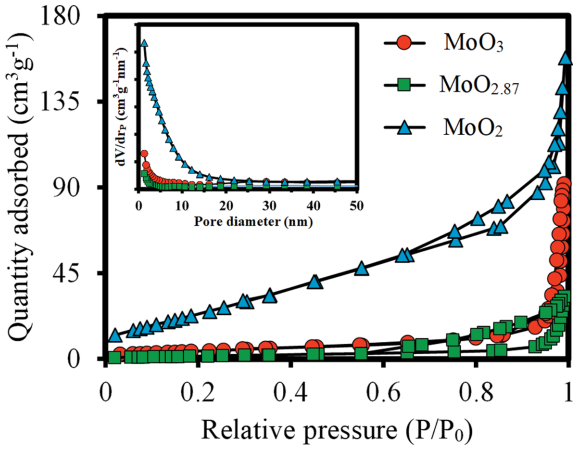



**Fig. 5. $N_2$ adsorption-desorption spectra of (a) $MoO_3$, (b) $MoO_{2.87}$, (c) and (d) $MoO_2$ samples (Inset: corresponding pore size distribution curves).**

**Table 1. BET surface area, pore volume and pore diameter of the samples**

| Sample | $S_{BET}$ ($m^2g^{-1}$) | Pore volume ($cm^3g^{-1}$) | Pore diameter (nm) |
|---|---|---|---|
| $MoO_3$ | 15.64 | 0.14 | 36.07 |
| $MoO_{2.87}$ | 5.94 | 0.05 | 33.04 |
| $MoO_2$ | 87.62 | 0.23 | 10.56 |

UV to NIR, which is suggested to be due to its metallic property [21]. Previous reports indicated the overlap of the conduction band and valance band of $MoO_2$, which exhibits the Fermi level lies inside the conduction band. As a result, the strong absorption of $MoO_2$ in visible and NIR can be attributed to localized surface plasmon resonance (SPR) of free d-electrons [21,37].

Fig. 5 presents the $N_2$ adsorption-desorption isotherms and pore size distribution curves of the $MoO_3$, $MoO_{2.87}$ and $MoO_2$ samples. It is observed the isotherms of all samples display a type IV isotherm with an $H_3$ hysteresis loop, indicating the presence of mesoporous structures [22,38]. As shown in Table 1, the specific surface area of $MoO_3$, $MoO_{2.87}$ and $MoO_2$ samples calculated by the BET method is 15.64, 5.94 and 87.62 $m^2g^{-1}$, respectively. In addition, the volume of adsorbed $N_2$ by $MoO_3$, $MoO_{2.87}$ and $MoO_2$ samples at relative pressure of 1.0 is 91.84, 32.88 and 157.92 $cm^3g^{-1}$, respectively. Thus, the $MoO_2$ sample displays much higher specific surface area and much stronger absorbability toward $N_2$ than the $MoO_3$ and $MoO_{2.87}$, suggesting that the $MoO_2$ can provide more active surface sites for adsorption of dye molecules. As shown in the inset of Fig. 6, the BJH method was also applied to determine the pore size distribution. It can be seen all the samples show a narrow pore size distribution ($r_p$<10 nm) with the peaks centered at ~1.29 nm.

## 2. Adsorption Performance

### 2-1. Adsorption Properties and their Kinetics for RhB Removal

The dye adsorption capability of products was investigated for removal of RhB molecules from water. Fig. S1(a)-(c) displays the temporal evaluation of absorption spectra of the RhB solution in

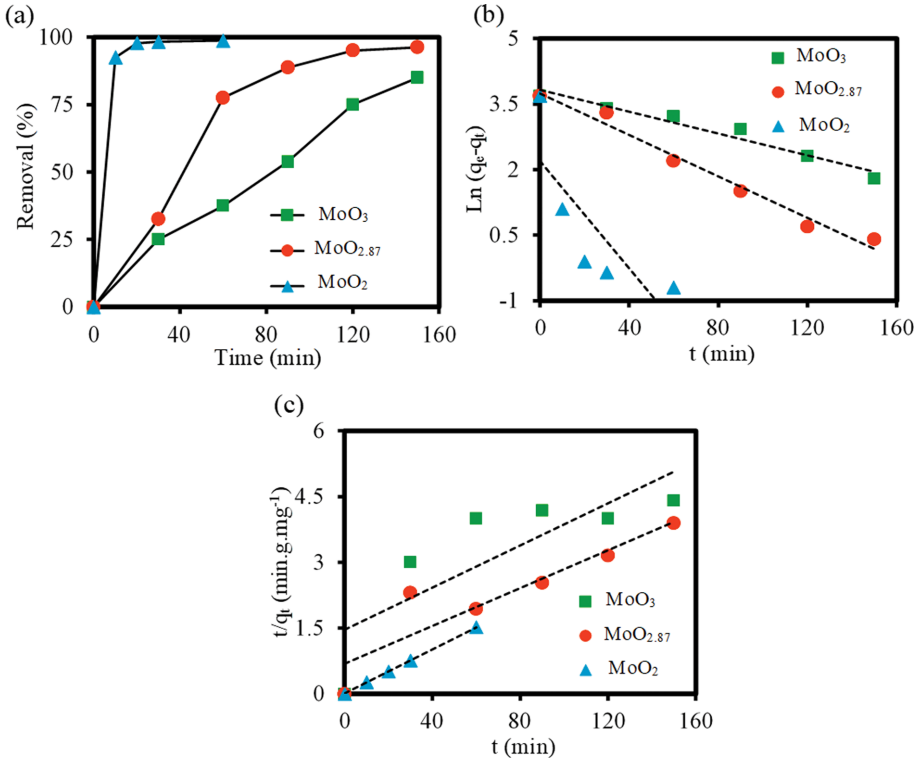



**Fig. 6. (a) The percentage removal, and the corresponding (b) pseudo first-order and (c) pseudo second-order kinetic models for the adsorption of RhB (45 mL, 40 mg/L) on the powder samples (45 mg).**

the presence of different adsorbents. It is observed that the intensity of the characteristic peak of RhB centered at 554 nm gradually decreases with increasing adsorption time, which indicates the removal of RhB molecules from water due to adsorption on the adsorbent. It can be seen the RhB adsorption onto $MoO_2$ is much faster than that of other samples. Fig. 6(a) shows the removal percentage for the RhB adsorption of samples. It is observed that nearly all the RhB molecules adsorbed onto $MoO_2$ nanoparticles within 20 min, while nearly 96% and 85% of RhB adsorbed onto $MoO_{2.87}$ nanoparticles and $MoO_3$ nanorods within 150 min, respectively. Therefore, the adsorption rate of RhB onto $MoO_2$ is much faster than that of $MoO_3$ and $MoO_{2.87}$.

The adsorption kinetics were studied to determine the adsorption rate and mechanism of RhB adsorption onto the products. To determine the adsorption mechanism of RhB, the pseudo-first-order and pseudo-second-order were fitted to the experimental data [39,40]. These models described as below [5,17]:

$$\ln(q_e - q_t) = \ln q_e - k_1 t \quad (3)$$

$$\frac{t}{q_t} = \frac{1}{k_2 q_e^2} + \frac{t}{q_e} \quad (4)$$

where $q_e$ (mg/g) and $q_t$ (mg/g) are the amount of RhB adsorbed at equilibrium and at various times, respectively, t is the adsorption time and $k_1$ and $k_2$ are the firs-order and second-order rate constants for RhB adsorption, respectively. As shown in Fig. 6(b) and (c), the experimental adsorption kinetics data were fitted by above two kinetic models. The corresponding kinetic parameters and the correlation coefficient parameters are summarized in Table 2. It can be seen the kinetic of RhB adsorption onto $MoO_2$ nanoparticles is better fitted by pseudo-second-order model. In contrast, the pseudo-first-order model is more suitable for RhB adsorption on $MoO_3$ and $MoO_{2.87}$ samples. As a result, the chemical adsorption is the rate-limiting step for RhB adsorption of $MoO_2$, while the RhB adsorption on $MoO_3$ and $MoO_{2.87}$ is more physical adsorption [11].

**Table 2. Adsorption kinetic parameters and isotherm parameters for the adsorption of RhB onto the samples**

| 1. Kinetic | | | | | | |
|---|---|---|---|---|---|---|
| | First-order | | | Second-order | | |
| | $k_1$ | $q_e$ | $R^2$ | $k_2$ | $q_e$ | $R^2$ |
| $MoO_3$ | 0.013 | 45.663 | 0.955 | 0.0004 | 41.666 | 0.651 |
| $MoO_{2.87}$ | 0.024 | 42.266 | 0.979 | 0.0007 | 42.296 | 0.835 |
| $MoO_2$ | 0.062 | 9.068 | 0.628 | 0.0803 | 39.682 | 0.999 |
| 2. Isotherm | | | | | | |
| | Langmuir | | | Freundlich | | |
| | $q_m$ | $k_L$ | $R^2$ | $K_F$ | 1/n | $R^2$ |
| $MoO_3$ | 169 | 1.552 | 0.997 | 60.273 | 0.127 | 0.930 |
| $MoO_{2.87}$ | 152 | 0.971 | 0.996 | 33.371 | 0.3253 | 0.925 |
| $MoO_2$ | 256 | 0.328 | 0.997 | 102.135 | 0.1931 | 0.896 |

2-2. Adsorption Isotherms

The adsorption behavior of $MoO_3$ nanorods, $MoO_{2.87}$ nanoparticles and $MoO_2$ nanoparticles was also investigated toward adsorp-

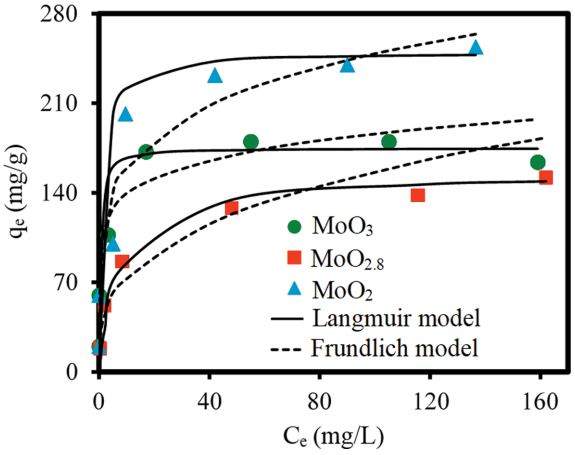



**Fig. 7. Fitting adsorption isotherms data for RhB adsorption on (a) $MoO_3$, (b) $MoO_{2.87}$ and (c) $MoO_2$ samples with Langmuir and Freundlich models.**

tion of RhB by fitting experimental data in equilibrium state to Langmuir and Freundlich models. The Langmuir assumes that all the adsorption surface sites are homogeneous and a monolayer is formed during dye adsorption. While, the Freundlich model described heterogeneous surface sites, which multilayer of adsorbed sites occurred during adsorption process [40,41]. The Langmuir (Eq. (5)) and Freundlich (Eq. (6)) models are described as below [5,17]:

$$\frac{C_e}{q_e} = \frac{1}{q_m K_L} + \frac{C_e}{q_m} \tag{5}$$

$$\mathrm{Ln}(q_e) = \mathrm{Ln}(K_F) + \frac{1}{n}\mathrm{Ln}(C_e) \tag{6}$$

where $q_e$ (mg/g) is the amount of RhB adsorbed at equilibrium, $q_m$ is the maximum adsorption capacity, $C_e$ (mg/L) is the concentration of RhB at equilibrium, $K_L$ is the Langmuir constant, $K_F$ is the Freundlich constant and 1/n is the intensity of adsorption. Fig. 7 and Fig. S2 show the fitting of Langmuir and Freundlich isotherms models to the experimental data obtained from adsorption of RhB with different concentration onto $MoO_3$, $MoO_{2.87}$ and $MoO_2$ samples in equilibrium states. The adsorption kinetic parameters are summarized in Table 2. From these data, it can be seen the adsorption of RhB onto all samples follows the Langmuir isotherm

**Table 3. The maximum adsorption capacity of different adsorbents**

| Adsorbent | Dye | $q_m$ (mg/g) | References |
|---|---|---|---|
| $MoS_2$ - nanosheets | MB | 146.43 | [40] |
| $SnS_2$ - Hierarchical | RhB | 200 | [5] |
| $MoS_2$ - Flower like | RhB | 291 | [39] |
| $W_{18}O_{49}$ - Nanowire | RhB | 120 | [42] |
| $MoO_3$ - hierarchical | RhB | 204 | [14] |
| $MoO_3$ - Nanoparticles | MB | 152 | [43] |
| $MoO_2$ - Hollow microspheres | Cr (VI) | 55 | [25] |
| $MoO_2$ - nanoparticles | RhB | 256 | This work |

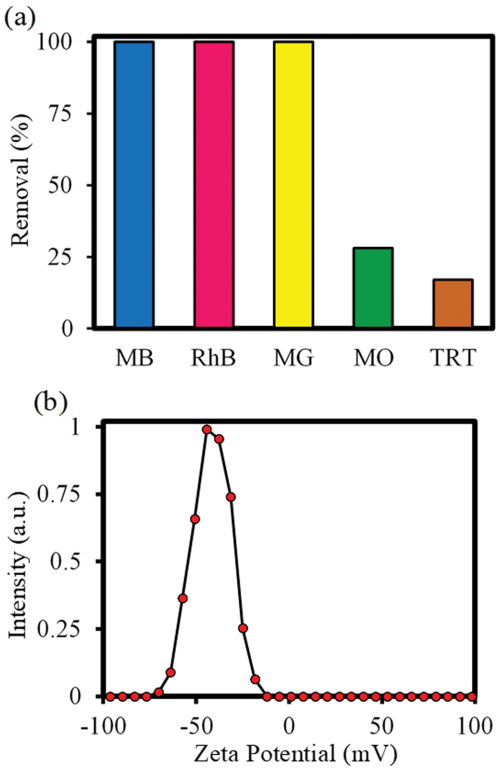



**Fig. 8. (a) The adsorption ability of $MoO_2$ nanoparticles to remove various organic dyes from aqueous solution (10 mg within 40 ml (10 mg/L)), and (b) zeta potential of $MoO_2$ nanoparticles.**

model. Based on this model, the maximum adsorption capacity of $MoO_3$, $MoO_{2.87}$ and $MoO_2$ is estimated to be 169, 152 and 256 mg/g, respectively. Thus, the maximum adsorption capacity of $MoO_2$ nanoparticles is higher than the previous reported values as shown in Table 3.

2-3. Selective Adsorption Ability

The adsorption ability of $MoO_2$ nanoparticles to remove other organic dyes from water was also investigated. In each experiment, 10 mg of $MoO_2$ sample was dispersed in 40 ml of various dyes with an initial concentration of 10 mg/L. Fig. 8(a) shows the adsorption ability of $MoO_2$ nanoparticles toward other dyes. It is observed the $MoO_2$ nanoparticles display excellent adsorption ability toward MB, RhB and MG as cationic dyes with the removal percentage of ~100%, while the values for MO and TRT as anionic dyes are 28% and 17%, respectively. Zeta potential measurement was carried out to determine the surface charge of nanoparticles. As shown in Fig. 8(b), the zeta potential is negative (−11.5 mV), which exhibits the negative surface charge of $MoO_2$ nanoparticles. As a result, the $MoO_2$ nanoparticles display more adsorption capability toward cationic dyes.

2-4. The Effect of pH and Temperature

It is well known that the initial pH of the dye solution and treatment temperature are important factors that may greatly affect the adsorption performance of metal oxides toward dye molecules. Thus, the effect of initial pH value and the treatment temperature on the removal properties of RhB on $MoO_2$ sample were also investigated. As shown in Fig. 9(a), the RhB can effectively remove from

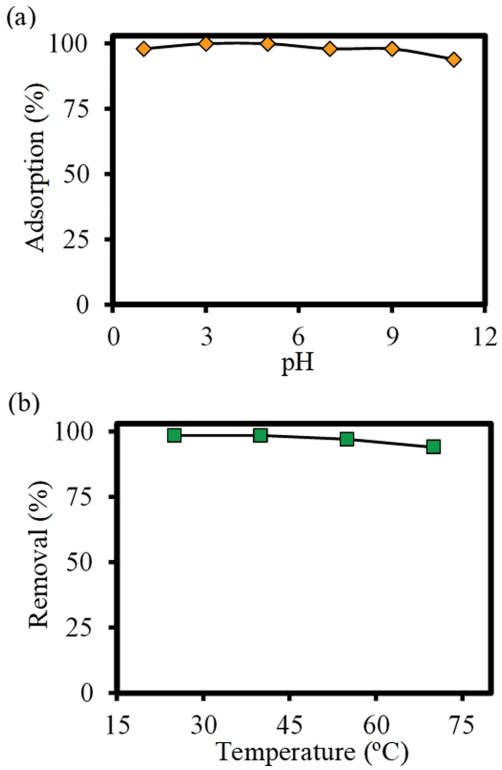



**Fig. 9. The effect of (a) initial pH and (b) temperature on the removal performance of RhB on $MoO_2$ nanoparticles.**

the water in the pH range of 1 to 11, and the pH has little effect on RhB adsorption performance. Moreover, the adsorption performance of the $MoO_2$ nanoparticles for RhB is nearly the same from 25-70 °C (Fig. 9(b)). These results reveal the importance of $MoO_2$ nanoparticles for practical application.

2-5. The Interaction between $MoO_2$ and RhB

An FTIR analysis was performed to determine the interaction between RhB and $MoO_2$. Fig. 10 shows the FTIR spectra of $MoO_2$ before and after RhB adsorption and pure RhB. It is observed the $MoO_2$ after RhB adsorption displays the characteristic peaks of RhB at 678 and in the spectral range of 1,000 $cm^{-1}$ to 1,700 $cm^{-1}$,

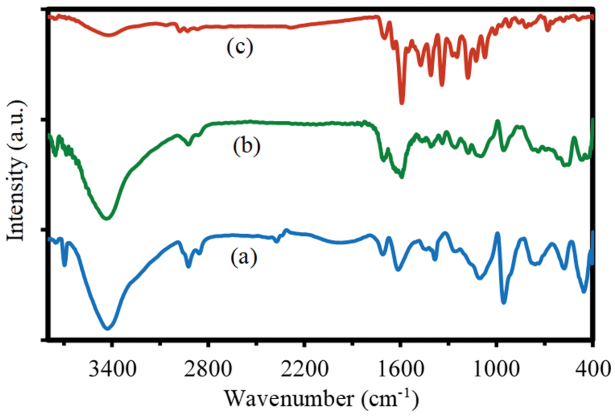



**Fig. 10. FTIR spectra of $MoO_2$ (a) before and (b) after adsorption of RhB, and (c) pure RhB.**

which confirms the RhB adsorption on $MoO_2$ nanoparticles. Moreover, the change in the intensity of FTIR peaks before and after RhB adsorption proposes the interaction between RhB and $MoO_2$.

## CONCLUSION

$MoO_3$ and reduced molybdenum oxides ($MoO_{2.87}$ and $MoO_2$) were successfully synthesized through a facile one-step hydrothermal method without and with the assistance of polymeric surfactants (PVP and PVA, respectively) as capping and reducing agents. It was found that the synthesized sample in the absence of polymeric surfactant is composed of orthorhombic phase of $MoO_3$ nanorods, while the monoclinic phases of $MoO_{2.87}$ nanoparticles and $MoO_2$ nanoparticles are formed with adding PVP and PVA as surfactant, respectively. Results indicated that the $MoO_2$ nanoparticles exhibit excellent ability for the rapid and efficient adsorption of organic dye from aqueous solution compared with $MoO_3$ and $MoO_{2.87}$. Nearly all the RhB molecules adsorbed onto $MoO_2$ nanoparticles within 20 min, while 96% and ~85% of RhB adsorbed onto $MoO_{2.87}$ and $MoO_3$ nanorods within 150 min. In addition, the maximum adsorption capacity of $MoO_2$ was estimated to be 256 mg/g, which is much larger than 169 and 152 $mgg^{-1}$ of $MoO_3$ and $MoO_{2.87}$ samples, respectively. The higher and rapid adsorption of RhB onto $MoO_2$ compared with $MoO_3$ and $MoO_{2.87}$ could be attributed to the larger specific surface area. The specific surface area of $MoO_2$ is 86.62 $m^2g^{-1}$, much larger than 15.64 and 5.94 $m^2g^{-1}$ of $MoO_3$ and $MoO_{2.87}$, respectively. The kinetic of RhB adsorption onto $MoO_2$ nanoparticles is better fitted by pseudo-second-order model. While, the pseudo-first-order model is more suitable for RhB adsorption on $MoO_3$ and $MoO_{2.87}$ samples. Furthermore, the adsorption of RhB onto all the samples follows the Langmuir isotherm model.

## SUPPORTING INFORMATION

Additional information as noted in the text. This information is available via the Internet at http://www.springer.com/chemistry/journal/11814.

## REFERENCES

1. A. J. Cramer and J. M. Cole, *J. Mater. Chem. A*, **5**, 10746 (2017).
2. K. Natarajan, H. C. Bajaj and R. J. Tayade, *J. Ind. Eng. Chem.*, **34**, 146 (2016).
3. S. Adhikari, S. Mandal, D. Sarkar, D. H. Kim and G. Madras, *Appl. Surf. Sci.*, **420**, 472 (2017).
4. X. Liu, W. Gong, J. Luo, C. Zou, Y. Yang and S. Yang, *Appl. Surf. Sci.*, **362**, 517 (2016).
5. S. Wang, B. Yang and Y. Liu, *J. Colloid Interface Sci.*, **507**, 225 (2017).
6. M. Toor and B. Jin, *Chem. Eng. J.*, **187**, 79 (2012).
7. L. P. Li, J. K. Kwan and K. L. Yeung, *Chem. Eng. J.*, **368**, 10 (2019).
8. T. Arumugham, R. G. Amimodu, N. J. Kaleekkal and D. Rana, *J. Environ. Sci. (China)*, **82**, 57 (2019).
9. N. Tahmasebi, S. Mirzavand, A. Hakimyfard and S. Barzegar, *Adv. Powder Technol.*, **30**, 257 (2019).
10. S. Adhikari and D. H. Kim, *Korean J. Chem. Eng.*, **36**, 468 (2019).
11. S. Zhang, H. Yang, H. Huang, H. Gao, X. Wang, R. Cao, J. Li, X. Xu

and X. Wang, *J. Mater. Chem. A*, **5**, 15913 (2017).
12. S. M. Ryu and C. Nam, *Phys. Status Solidi (a)*, **215**, 1700996 (2018).
13. S. Jeon and K. Yong, *J. Mater. Chem.*, **20**, 10146 (2010).
14. M. Wang, X. X. Song, X. L. Cheng, X. Zhou, X. F. Zhang, Z. Cai, Y. M. Xu, S. Gao, H. Zhao and L. H. Huo, *RSC Adv.*, **5**, 85248 (2015).
15. L. Xiao, S. Zhang and J. Huang, *Powder Technol.*, **258**, 297 (2014).
16. W. Mu, M. Li, X. Li, Z. Ma, R. Zhang, Q. Yu, K. Lv, X. Xie, J. He, H. Wei and Y. Jian, *Dalton Trans.*, **44**, 7419 (2015).
17. K. Lin, M. Qin, X. Geng, L. Wang and H. Wu, *Adv. Powder Technol.*, **29**, 1933 (2018).
18. N. Wang, J. Chen, J. Wang, J. Feng and W. Yan, *Powder Technol.*, **347**, 93 (2019).
19. Y. Zhan, Y. Liu, H. Zu, Y. Guo, S. Wu, H. Yang, Z. Liu, B. Lei, J. Zhuang, X. Zhang and D. Huang, *Nanoscale*, **10**, 5997 (2018).
20. Q. Huang, S. Hu, J. Zhuang and X. Wang, *Chem. Eur. J.*, **18**, 15283 (2012).
21. Q. Zhang, X. Li, W. Yi, W. Li, H. Bai, J. Liu and G. Xi, *Anal. Chem.*, **89**, 11765 (2017).
22. Y. Zhao, Y. Zhang, Z. Yang, Y. Yan and K. Sun, *Sci. Technol. Adv. Mat.*, **14**, 043501 (2013).
23. X. Li, J. Shao, J. Li, L. Zhang, Q. Qu and H. Zheng, *J. Power Sources*, **237**, 80 (2013).
24. W. Liu, X. Li, W. Li, Q. Zhang, H. Bai, J. Li and G. Xi, *Biomaterials*, **163**, 43 (2018).
25. H. Hu, J. Xu, C. Deng and X. Ge, *Mater. Res. Bull.*, **51**, 402 (2014).
26. Z. Hu, G. Liu, X. Chen, Z. Shen and J. C. Yu, *Adv. Funct. Mater.*, **26**, 4445 (2016).
27. Y. Cao, H. Wang, X. Ren, F. Li, J. Wang, R. Ding, L. Wang, J. Wu, Z. Liu and B. Lv, *CrystEngComm*, **21**, 5106 (2019).
28. K. M. Koczkur, S. Mourdikoudis, L. Polavarapu and S. E. Skrabalak, *Dalton Trans.*, **44**, 17883 (2015).
29. P. Sagitha, K. Sarada and K. Muraleedharan, *Trans. Nonferrous Met. Soc. China*, **26**, 2693 (2016).
30. I. Washio, Y. Xiong, Y. Yin and Y. Xia, *Adv. Mater.*, **18**, 1745 (2006).
31. C. V. S. Reddy, E. H. Walker, S. A. Wicker, Q. L. Williams and R. R. Kalluru, *J. Solid State Electr.*, **13**, 1945 (2009).
32. A. S. Etman, H. N. Abdelhamid, Y. Yuan, L. Wang, X. Zou and J. Sun, *ACS Omega*, **3**, 2193 (2018).
33. C. V. S. Reddy, Y. Y. Qi, W. Jin, Q. Y. Zhu, Z. R. Deng, W. Chen and S. I. Mho, *J. Solid State Electr.*, **11**, 1239 (2007).
34. R. S. Patil, M. D. Uplane and P. S. Patil, *Appl. Surf. Sci.*, **252**, 8050 (2006).
35. H. Zhang, L. Zeng, X. Wu, L. Lian and M. Wei, *J. Alloys Compd.*, **580**, 358 (2013).
36. A. Kharazmi, N. Faraji, R. M. Hussin, E. Saion, W. M. M. Yunus and K. Behzad, *Beilstein J. Nanotechnol.*, **6**, 529 (2015).
37. Y. Zhang, K. Sun, D. Wu, W. Xie, F. Xie, X. Zhao and X. Wang, *ChemCatChem*, **11**, 2546 (2019).
38. H. Song, S. You and X. Jia, *Appl. Phys. A.*, **121**, 541 (2015).
39. S. Han, K. Liu, L. Hu, F. Teng, P. Yu and Y. Zhu, *Sci. Rep.*, **7**, 43599 (2017).
40. X. Q. Qiao, F. C. Hu, F. Y. Tian, D. F. Hou and D. S. Li, *RSC Adv.*, **6**, 11631 (2016).
41. Z. Li, X. Meng and Z. Zhang, *Mater. Res. Bull.*, **111**, 238 (2019).
42. X. Gao, F. Xiao, C. Yang, J. Wang and X. Su, *J. Mater. Chem. A*, **1**, 5831 (2013).
43. S. Rakass, H. O. Hassani, M. Abboudi, F. Kooli, A. Mohmoud, A. Aljuhani and F. Al Wadaani, *Molecules*, **23**, 2295 (2018).

# Supporting Information

# Synthesis of $MoO_x$ nanostructures with the assistance of polymeric surfactants for dye removal from water

**Nemat Tahmasebi[†] and Marzieh Khalildashti**

Department of Physics, Jundi-Shapur University of Technology, Dezful, Iran
(*Received 5 September 2019 • accepted 21 December 2019*)

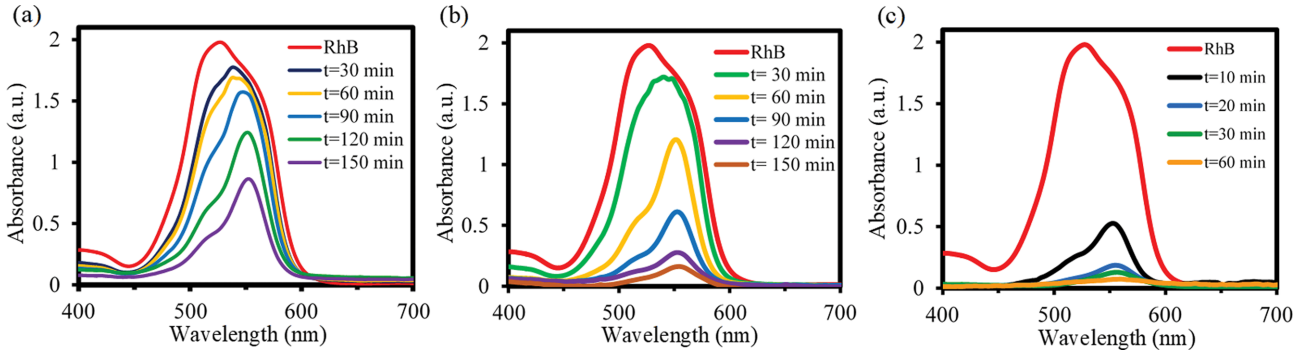



**Fig. S1. The temporal evaluation of absorption spectra of the RhB solution (45 mL, 40 mg/L) in the presence of 45 mg of (a) $MoO_3$, (b) $MoO_{2.87}$ and (c) $MoO_2$.**

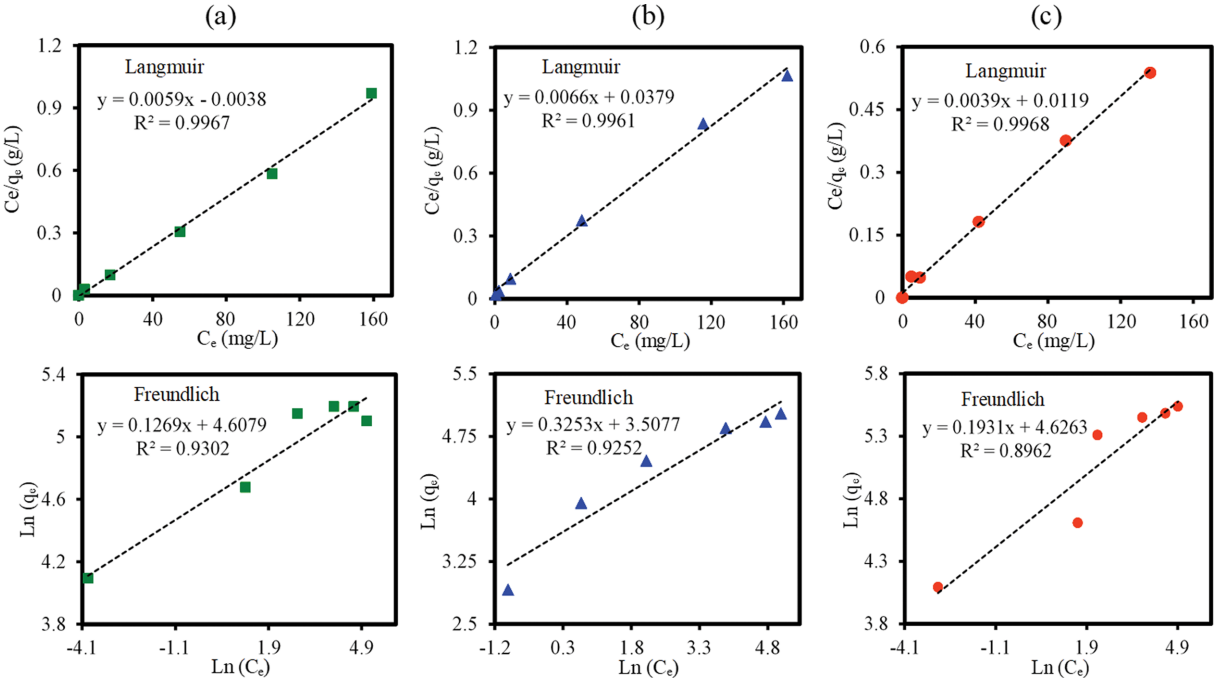



**Fig. S2. The fitting of Langmuir and Freundlich isotherms models to the experimental data obtained from adsorption of RhB with different concentration onto (a) $MoO_3$, (b) $MoO_{2.87}$ and (c) $MoO_2$ samples in equilibrium states.**